

In-vivo Fourier domain optical coherence tomography as a new tool for investigation of vasodynamics in the mouse model

Sven Meissner

University of Technology, Dresden
Clinical Sensing and Monitoring
Faculty of Medicine Carl Gustav Carus
Fetscherstrasse 74
Dresden, 01307
Germany

Gregor Müller

University of Technology, Dresden
Department of Vascular Endothelium and Microcirculation
Faculty of Medicine Carl Gustav Carus
Fetscherstrasse 74
Dresden, 01307
Germany

Julia Walther

University of Technology, Dresden
Clinical Sensing and Monitoring
Faculty of Medicine Carl Gustav Carus
Fetscherstrasse 74
Dresden, 01307
Germany

Henning Morawietz

University of Technology, Dresden
Department of Vascular Endothelium and Microcirculation
Faculty of Medicine Carl Gustav Carus
Fetscherstrasse 74
Dresden, 01307
Germany

Edmund Koch

University of Technology, Dresden
Clinical Sensing and Monitoring
Faculty of Medicine Carl Gustav Carus
Fetscherstrasse 74
Dresden, 01307
Germany

1 Introduction

Cardiovascular disease is the major cause of death in the industrialized world.¹ Cardiovascular risk factors and inflammation can ultimately lead to life-threatening complications²⁻⁴ by contributing to endothelial dysfunction and atherosclerotic plaque formation on vessel walls.^{5,6} Impaired vasodynamics is considered to be a symptom of early atherosclerotic changes in the vessel wall. Such changes limit the response to vasoactive stimuli and increase vascular stiffness.⁷ Current vasody-

Abstract. *In-vivo* imaging of the vascular system can provide novel insight into the dynamics of vasoconstriction and vasodilation. Fourier domain optical coherence tomography (FD-OCT) is an optical, non-contact imaging technique based on interferometry of short-coherent near-infrared light with axial resolution of less than 10 μm . In this study, we apply FD-OCT as an *in-vivo* imaging technique to investigate blood vessels in their anatomical context using temporally resolved image stacks. Our chosen model system is the murine saphenous artery and vein, due to their small inner vessel diameters, sensitive response to vasoactive stimuli, and advantageous anatomical position. The vascular function of male wild-type mice (C57BL/6) is determined at the ages of 6 and 20 weeks. Vasoconstriction is analyzed in response to dermal application of potassium (K^+), and vasodilation in response to sodium nitroprusside (SNP). Vasodynamics are quantified from time series (75 sec, 4 frames per sec, 330×512 pixels per frame) of cross sectional images that are analyzed by semiautomated image processing software. The morphology of the saphenous artery and vein is determined by 3-D image stacks of $512 \times 512 \times 512$ pixels. Using the FD-OCT technique, we are able to demonstrate age-dependent differences in vascular function and vasodynamics. © 2009 Society of Photo-Optical Instrumentation Engineers. [DOI: 10.1117/1.3149865]

Keywords: vasodynamics; Fourier domain optical coherence tomography; atherosclerosis.

Paper 08283RR received Aug. 12, 2008; revised manuscript received Mar. 10, 2009; accepted for publication Apr. 8, 2009; published online Jun. 9, 2009. This paper is a revision of a paper presented at the SPIE conference on Optical Coherence Tomography and Coherence Techniques III, June 2007, Munich, Germany. The paper presented there appears (unrefereed) in SPIE Proceedings Vol. 6627.

dynamic studies are mainly performed by isometric force measurement of isolated vessels in organ chambers. This approach provides information about different parameters, e.g., concentration-response curves of pharmacological interventions, but only in the *ex-vivo* situation. To better understand the pathogenesis of atherosclerosis, *in-vivo* measurement of vasodynamics would be a useful diagnostic tool.

In-vivo measurement of vasodynamics is not well established for small vessels, because imaging techniques are limited by the high resolution needed. Current commercial ultrasound technology only provides a resolution of about 50 μm , which does not allow imaging of structures approximately

Address all correspondence to: Sven Meissner, Klinisches Sensing und Monitoring, Medizinische Fakultät der Technischen Universität Dresden, Fetscherstraße 74, 01307 Dresden, Germany. Tel: +49 351 458 6133; Fax: +49 351 458 6325; E-mail: Sven.Meissner@tu-dresden.de

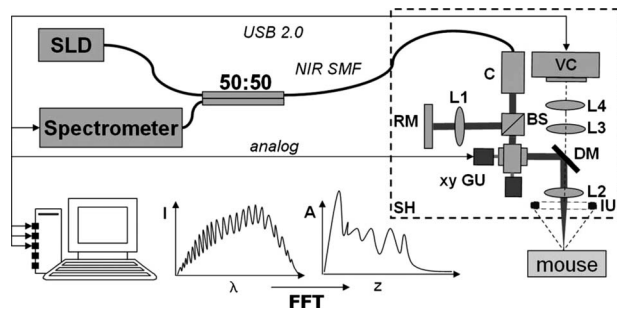


Fig. 1 Experimental setup to investigate *in-vivo* vasodynamics in the mouse model. Near-infrared (NIR) light is transmitted by fiber optics [single mode fiber (SMF)] and coupled by a collimator (C) with a focal length of 12 mm into the scanner head (SH). The light beam is divided by a beamsplitter (BS) cube into a reference and sample beam. The sample beam is then deflected by two galvanometer scanners (xy GU) into *x* and *y* directions for plane scanning of the sample. The sample beam is focused on the sample by an achromatic lens (L2) with a focal length of 25.4 mm. The reference light is focused L1 to the reference mirror (RM). Backscattered light from the sample is superimposed with the reference light at the beamsplitter cube. This interference signal is transmitted into the spectrometer and spectrally resolved by a diffraction grating (1200 lines/mm). The interference spectrum is acquired by a silicon line detector. Using a fast Fourier transformation (FFT), the interference signal is converted into the corresponding depth information. Additionally, in the course of the sample beam, a dichroic mirror (DM) is inserted for adaptation of a video camera (VC). Further abbreviations: IU is illumination unit for VC; λ is the wavelength; *z* is the depth; *I* is the Intensity; and *A* is log. Amplitude is in decibels.

100 μm in diameter. Optical coherence tomography (OCT)⁸ could be a suitable novel technique to measure vasodynamics in small vessels *in vivo* due to its contactless imaging and superior resolution of less than 10 μm . This high resolution of OCT facilitates the generation of 2-D cross sections and 3-D tomograms of subsurface tissue. Recently, intravascular catheter OCT has been used to characterize atherosclerotic plaque formation in human vessels.⁹ However, due to the large diameter of the catheters, this technique is not applicable to the small vessels in mouse models.

Here, we describe a novel *in-vivo* approach that allows high-speed transluminal studies of impaired vasodynamics in the mouse at early stages of atherosclerosis, before visible plaque formation. Transluminal imaging of the vessels has the advantage of avoiding microtraumata in the endothelium. Additionally, compared to established *ex-vivo* methods, our approach allows the vessels to remain in their proper anatomical and physiological context with continuous blood flow, blood pressure, and innervation.¹⁰

2 Methods and Materials

2.1 Experimental Setup

A Fourier domain OCT (FD-OCT)¹¹ system was developed with a center wavelength of 840 nm, a spectral width (FWHM) of 45 nm, and an optical power of 1 mW. A broadband superluminescent diode (SLD) served as the light source. Light was transmitted by a fiber coupler to the scanner head (Fig. 1), in which the light was collimated into a free-space beam of 2.4 mm in diameter ($1/e^2$) and divided by a beamsplitter cube into a reference and a sample beam. The

sample beam was deflected by two galvanometer scanners in the *x* and *y* direction. Deflected light was focused onto the sample by an achromatic lens (L2) with a focal length of 25.4 mm and a diameter of 15 mm. Because of the much larger diameter of L2 compared to the sample beam diameter, the effective NA of 0.05 of the objective is determined by the focal length of the collimator, the NA of the fiber, and the focal length of L2. Backscattered light from the probe was superimposed with the reference beam and again coupled into the single-mode fiber. Interfered light was coupled into the spectrometer by a collimator with a focal length of 40 mm, and was spectrally resolved by a diffraction grating with 1200 lines/mm before being focused onto the complimentary metal oxide semiconductor (CMOS) line detector (1024 pixels, $7.8 \times 125 \mu\text{m}$) by an achromatic lens with a 75-mm focal length. This OCT system allows the measurement of complex biological tissue in a range of 2 mm, with an axial resolution of 8 μm in air (6 μm in tissue with refractive index $n=1.33$), a lateral resolution of about 7 μm , and a scanning rate of 1.2 kHz (A-scan rate). Although the measurement range is 2 mm, its sensitivity range is limited to a range of 370 μm by the Rayleigh length of the sample beam. A schematic of the experimental setup and beam course in the scanner head is shown in Fig. 1. The camera, which is coupled by a dichroic mirror, allowed orientation on the sample surface, and can be used with additional optics for microscopy. Optimal position in relation to the sample was achieved by mounting the scanner head on a three-axis translation stage.

2.2 Mouse Model

All experiments were performed in accordance with the *Guide for the Care and Use of Laboratory Animals* (Institute of Laboratory Animal Resources, 7th edition, National Academy Press, Washington, D.C., 1996). The study was approved by the governmental animal care and use committee. The murine saphenous artery and vein of the right hind leg in C57BL/6 mice aged 6 or 20 weeks was investigated. Anesthesia was delivered by peritoneal application of a mixture of 95% Ketanest (10 mg/ml) and 5% Xylazin (20 mg/ml) using a dose of 10- $\mu\text{l/g}$ body weight. Before imaging, the skin covering the saphenous artery was incised and a $5 \times 5\text{-mm}^2$ skin flap was removed to obtain access to the vessel area. Phosphate-buffered saline (PBS) containing 80-mM K^+ was used to induce vasoconstriction (VC). Vasodilation (VD) was induced with 1-mM sodium nitroprusside solution (PBS+SNP). The solutions were applied on the outer vessel wall. During investigation, the mouse was fixed to a temperature-controlled operation table for small rodents.

2.3 Two-Dimensional Image Acquisition—Vasodynamics

Throughout the image acquisition procedure, the vessel-containing area was covered with buffer (PBS) to prevent the tissue from drying out. To measure vasodynamics, images of the inner vessel diameter were taken at identical lateral positions and recorded by performing B-scans consisting of 300 A-scans. An image acquisition rate of 4 B-scans per second was used. VC and VD were documented by initial 30 B-scans to determine the unaffected vessel diameter. Next, image ac-

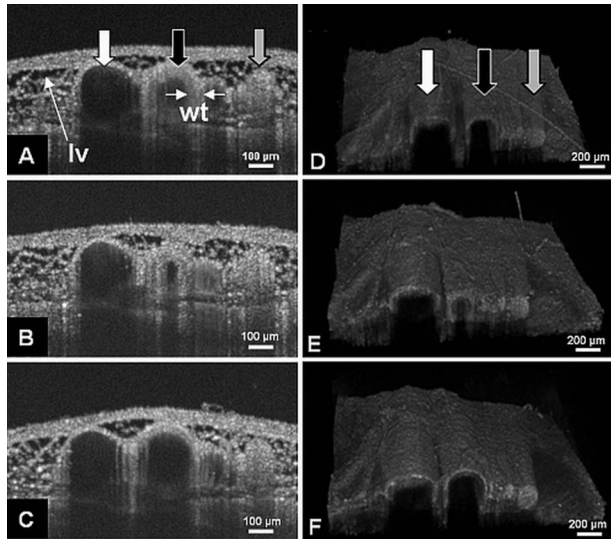


Fig. 2 (a), (b), and (c) 2-D cross sectional OCT images and (e) and (f) volume rendering illustrations of the investigated area under (a) and (d) control conditions, (b) and (e) VC, and (c) and (f) VD. The saphenous vein (white arrow), the saphenous artery (black arrow), and the *nervus vastus medialis* (gray arrow) are indicated. Vessel wall thickness wt of the saphenous artery is highlighted by double arrows. The resolution of our OCT system is sufficient to image the lipid-filled vacuoles of perivascular adipocytes (lv).

quisition was stopped and the buffer was exchanged for a buffer solution containing vasoactive stimuli (VC: PBS+K⁺; VD: PBS+SNP). Resultant changes in diameter were imaged by additional 300 B-scans. The final values of the inner diameter after VC and VD were determined using the last 50 images (equivalent to the last 12 sec of the time-resolved image stack) of the OCT image stack acquired during VC and VD. The time-resolved image stacks of the static and dynamic portion of each stimulus represent a period of approximately 75 sec.

2.4 Three-Dimensional Image Acquisition—Morphology

The investigated area was also mapped by 3-D image stacks ($2 \times 2 \times 2 \text{ mm}^3$), under control conditions and after completion of VC and VD.

2.5 Image Quantification

Flowing blood was seen in these OCT images as a specific black shadow, caused by the movement of scattering objects, e.g., blood cells. This movement reduced the interference signal by fringe washout.^{12,13} The saphenous artery was seen in OCT images as a black semicircular structure (Figs. 2 and 3). The pronounced border between the dark blood and bright vessel wall was used to quantify the inner diameter of the artery. Quantification was carried out using existing algorithms from commercially available software, National Instruments Vision Assistant 8.2.1 (NIV), in combination with National Instruments LabVIEW protocols. In the first B-scan of the time-resolved stack, the user defined the region of interest (ROI), which included the saphenous artery, by a rectangle. The border between the dark lumen and bright vessel wall was detected with NIV routine cycle detection. The protocol was modified to detect the visible semicircular structure representing the saphenous artery lumen. The inner diameter of the semicircle and the coordinates of the center point detected in the first B-scan diameter were used to define the ROI in the following B-scan. The ROI was defined by the user only in the first B-scan. All subsequent B-scans in the time-resolved image stack were analyzed automatically. The detected inner diameters and the corresponding times were saved as spreadsheet files. To characterize the dynamics of inner diameter change in response to vasoactive stimuli, a sigmoid function [Eq. (1)] was fitted to the measured dataset of time-dependent inner diameter $d(t)$. The coefficient Δd describes the total change of inner diameter, $t_{1/2}$ the elapsed time for half of inner diameter change, τ the time constant of diameter change, d_0 the initial diameter, and “ t ” the time.

$$d(t) = \Delta d [1 + \exp((t - t_{1/2})/\tau)]^{-1} + d_0. \quad (1)$$

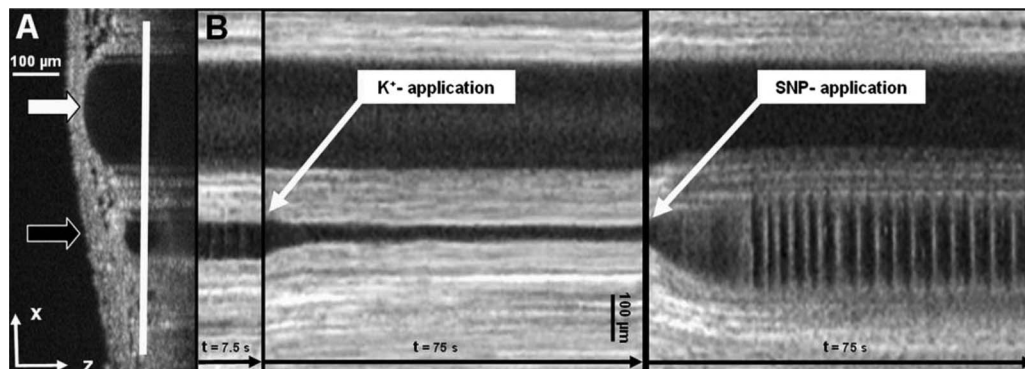


Fig. 3 Temporal changes of the inner diameter after induction of vasoconstriction (K⁺) and vasodilation (SNP). Left side: 2-D cross sectional OCT image taken at resting conditions of saphenous vein (white arrow) and saphenous artery (black arrow). Right: cross sectional images of the acquired time-resolved stacks. The white line in the left image marks the cutting plane through the time-resolved stacks. The temporal resolution of the inner diameter of the saphenous artery and vein are visible as black bands in the right image. After application of K⁺, the inner diameter decreases, whereas SNP application enlarges the vessel diameter.

Vascular function dynamics were characterized by the time to half maximum $t_{1/2}$ (inflection point of the fitted function) during VC and VD, and the velocity of inner diameter change at the inflection point. The maximum velocity v_{\max} of VC and VD corresponds to the slope at $t=t_{1/2}$, where the second time derivative of Eq. (1) is null and is given by:

$$v_{\max} = \frac{|\Delta d|}{4 \cdot \tau}. \quad (2)$$

The wall thickness wt of the saphenous artery and vein was manually quantified using ImageJ software (ImageJ 1.37v). Statistical analysis was carried out with Graph Pad Prism 5 using the unpaired t-test.

3 Results

3.1 Morphology

To investigate *in-vivo* vascular function in small vessels, we chose the murine saphenous artery and vein of the right hind leg because of its advantageous anatomical position beneath the skin on the *musculus vastus medialis*, its suitable inner diameter of approximately 100 μm , and its rapid response to vasoactive stimuli. Figure 2(a) is a representative OCT gray-scale cross section of a murine artery and vein, as well as the surrounding tissue and other structures including nerves. The surrounding tissue consists of perivascular fat and appears as a foamy structure. Lipid containing vacuoles (lv; left arrow) in perivascular adipocytes (approximately 80 μm in diameter) are visible beneath the surface, which is represented by connecting tissue of muscle fascia. The distinctive ring structures encircling the vessel lumens are the arterial and venous vessel walls. Vessel wall thickness wt is indicated by a double arrow. The lumen and vessel wall of the saphenous vein (white arrow) and artery (black arrow), as well as the nerve (*nervus vastus medialis*; gray arrow), are shown under control conditions [Fig. 2(a)], and after VC [Fig. 2(b)] and VD [Fig. 2(c)]. Morphology is revealed by 3-D volume rendering of murine tissue containing the same structures before [Fig. 2(d)] and after VC [Fig. 2(e)] and VD [Fig. 2(f)].

3.2 Vasodynamics

The morphological vessel parameters used to characterize vessel dynamics of mice aged 6 (6w) and 20 (20w) weeks were: 1. the inner diameter d as determined from the blood-filled lumen confined by the vessel wall, and 2. the vessel wall thickness wt of the saphenous artery and vein. During vasoconstriction (VC) and vasodilation (VD), these parameters (d_{VC} , d_{VD} , wt_{VC} , and wt_{VD}) differ from resting conditions (d_{res} , wt_{res}). To define vessel reactions to vasoactive stimuli, we determined the dynamic range $dr=|d_{VD}-d_{VC}|$ and dynamic ratio (d_{VC}/d_{VD}) as a degree of vessel stiffness. The relative wall thickness $wt_{\text{rel}}=wt_{\text{res}}/(d_{\text{res}}/2)$ characterized the vessel type. In previous studies, the relative wall thickness of the aorta was characterized by a value of 0.2, which increased to 0.5 in arteries and to 1.0 in arterioles.¹⁴ This increase was found to be more moderate in the venous bloodstream, starting at 0.1 for the vena cava, 0.2 in veins, and 0.3 in venules. The maximum velocity v_{\max} of inner diameter change provides information about how fast the vessel reacts to vasoac-

tive stimuli, and the time to half maximum diameter change $t_{1/2}$ indicates how long it takes until these reactions are finished.

Changes in the inner diameter of the saphenous artery and vein during VC and VD were recorded in a quantitative manner using the FD-OCT technique (Table 1). Analyzing the saphenous vein, we detected only slight inner diameter and wall thickness changes between both age groups in response to vasoactive stimuli. In contrast, the inner diameter of the saphenous artery of 6-week-old mice altered from $122 \pm 6 \mu\text{m}$ under resting conditions to $10 \pm 3 \mu\text{m}$ after VC (d_{VC}) and $227 \pm 4 \mu\text{m}$ after VD (d_{VD}). At 20 weeks of age, the inner diameter of the saphenous artery had increased due to the growth of the animal to $172 \pm 9 \mu\text{m}$ (resting conditions), $38 \pm 7 \mu\text{m}$ (d_{VC}), and $245 \pm 8 \mu\text{m}$ (d_{VD}). While the dynamic range of the vessel diameter did not change with age (6w= $217 \pm 5 \mu\text{m}$ and 20w= $207 \pm 9 \mu\text{m}$), the vessel wall stiffness increased significantly by a factor of 4 from 0.04 ± 0.01 (6w) to 0.16 ± 0.03 after 20 weeks of age. In both age groups, the arterial vessel wall was always thicker than the venous vessel wall. Arterial wall thickness in 6-week-old mice increased from $24 \pm 1 \mu\text{m}$ at resting conditions to $38 \pm 2 \mu\text{m}$ after VC, and decreased to $18 \pm 1 \mu\text{m}$ after VD. In 20-week-old mice, wt changed from $22 \pm 1 \mu\text{m}$ during resting conditions to $46 \pm 2 \mu\text{m}$ after VC and $18 \pm 1 \mu\text{m}$ after VD. The wt_{VC} and wt_{rel} of 6-week-old mice showed significant differences compared to 20-week-old animals. The relative wall thickness wt_{rel} of the arteries changed from a value of 0.44 (6w) to 0.27 (20w). The measured wt_{rel} for arteries is in the range of the relative wall thickness described in the literature.¹⁴

Figure 3 shows a representative image of changes in the saphenous artery inner diameter over time (black arrow). Here, cross sections from the time-resolved image stacks under control, VC, and VD conditions were sequentially combined to clearly demonstrate inner diameter changes after the application of vasoactive stimuli. In the saphenous artery lumen, an alternating light and dark pattern was observed after VD. This likely represents the detection of blood cells with reduced flow velocity during the diastolic part of the cardiac cycle by the OCT system.

Figure 4 shows an example of changes in the saphenous artery inner diameter during VC and the corresponding graph of the fitted sigmoid function. Inner diameter was determined by the algorithm described in the image quantification section of the methods. The dynamic parameters v_{\max} and $t_{1/2}$ during VC and VD for the saphenous arteries in each age cohort are shown in Table 2. Dynamic responses were not detectable for the saphenous vein. Although the reaction velocity (v_{\max}) was faster in response to VD than VC in both age groups, comparison of $t_{1/2}$ indicates that VC progressed more rapidly (6w= 4.5 ± 0.4 s; 20w= 6.5 ± 0.4 s) than VD (6w= 8.5 ± 1.2 s; 20w= 9.8 ± 0.5 s).

4 Discussion and Conclusion

Here we demonstrate that FD-OCT is a novel technique that is highly suitable for *in-vivo* investigation of the vasodynamics of arteries and veins in the mouse model. We show that FD-OCT facilitates contactless imaging of the saphenous artery and vein with 2-D cross sectional images and 3-D tomograms.

Table 1 Quantification of the inner diameter d and vessel wall thickness wt of the saphenous artery and vein under resting condition d_{res} and wt_{res} , after vasoconstriction (VC) d_{VC} and wt_{VC} , and after vasodilation (VD) d_{VD} and wt_{VD} . Dynamic range $dr = |d_{VD} - d_{VC}|$ and dynamic ratio d_{VC}/d_{VD} , and the relative wall thickness $wt_{rel} = wt_{res}/(d_{res}/2)$ were compared between mice aged 6 (6w) and 20 (20w) weeks. * $p < 0.05$; ** $p < 0.01$; *** $p < 0.001$ versus 6w.

	Artery		Vein	
	6w (n=30)	20w (n=14)	6w (n=30)	20w (n=14)
Inner diameter [μm]				
d_{res}	122 \pm 6	172 \pm 9***	225 \pm 8	208 \pm 10
d_{VC}	10 \pm 3	38 \pm 7***	224 \pm 6	221 \pm 10
d_{VD}	227 \pm 4	245 \pm 8*	244 \pm 9	228 \pm 12
dr	217 \pm 5	207 \pm 8	25 \pm 7	17 \pm 6
d_{VD}/d_{VC}	0.04 \pm 0.01	0.16 \pm 0.03***	0.93 \pm 0.03	0.98 \pm 0.03
Wall thickness [μm]				
wt_{res}	23.9 \pm 0.8	22.0 \pm 1.1	16.8 \pm 0.5	16.1 \pm 0.5
wt_{VC}	37.6 \pm 1.7	46.1 \pm 1.7**	17.3 \pm 0.6	16.5 \pm 0.9
wt_{VD}	18.3 \pm 0.8	17.7 \pm 1.0	15.4 \pm 0.7	14.3 \pm 0.9
Relative wall thickness				
wt_{rel}	0,44 \pm 0.03	0.27 \pm 0.02***	0.15 \pm 0.01	0.16 \pm 0.01

FD-OCT allows quantification of vessel wall thickness and inner diameter of the saphenous artery and vein, and is a means to follow the time course of inner diameter change during VC and VD. Importantly, FD-OCT mediated analysis largely leaves physiological parameters such as blood flow, blood pressure, and neural innervations intact. It also has the advantage of avoiding the preparation trauma associated with traditional methods that rely on isometric force measurements of vessel rings in organ chambers. Use of FD-OCT *in vivo* in the mouse represents a novel opportunity to investigate vasodynamics in a physiological context.

We demonstrate that the resolution and A-scan rate of our FD-OCT system are sufficient to detect significant differences in inner vessel diameter and wall thickness. FD-OCT has an advantage over wire myography because it allows replicate interventions, as evidenced by our analysis of the same animals at 6 and 20 weeks of age. This offers the opportunity to analyze long-term changes in the vasculature and to study, e.g., pharmaceutical effects, over a time course without sacrificing the animals.¹⁵ Our detection of physiological changes in vessel wall thickness in response to vasoactive stimuli agrees with previous histological investigations.¹⁶ The observed progressive limitation of vessel dynamics might be able to facilitate the genesis of cardiovascular diseases caused by reduced elasticity of the vessel wall. Especially during systolic peak pressure, the limited elasticity of the vessel wall results in an increased wall tension, and finally leads to an endothelial dysfunction and cardiovascular disease in old age.

In conclusion, we demonstrate that our FD-OCT system with an A-scan rate of 1.2 kHz allows vasodynamics in murine vasculature to be quantified with an improved temporal

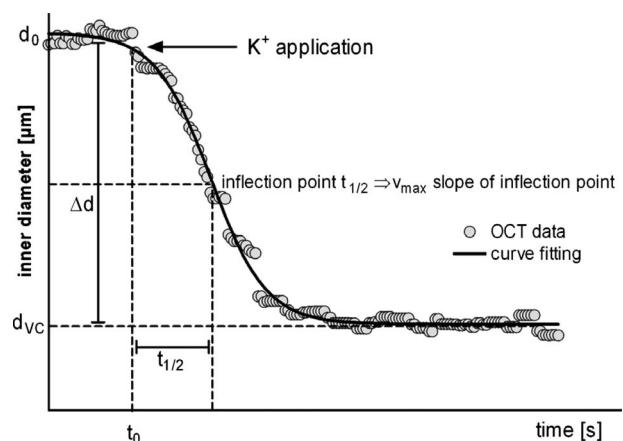


Fig. 4 Time course of inner diameter change during vasoconstriction (VC) measured by FD-OCT (gray circles) and the fitted sigmoid function (black line). At time t_0 , the vasoconstrictor K^+ was applied. Δd indicates the change from the initial inner diameter d_0 to the final inner diameter d_{VC} during VC. The dynamics of inner diameter change were quantified using the time of half VC $t_{1/2}$ and the maximum velocity v_{max} of inner diameter change, reflecting the slope at the inflection point. VD dynamics were analyzed in a similar manner.

Table 2 Quantification of maximum velocity v_{\max} in $\mu\text{m/s}$ of inner diameter change and time to half maximum VC or VD $t_{1/2}$ in s during VC and VD in 6-week (6w) and 20-week-old (20w) mice. No dynamic behavior was detected in the saphenous vein (n.d.). ** $p < 0.01$ versus 6w.

v_{\max} [$\mu\text{m/s}$]	Artery		Vein	
	6w	20w	6w	20w
VC	16.1 \pm 2.0	14.6 \pm 1.4	n.d.	n.d.
VD	20.2 \pm 2.6	19.4 \pm 1.6	n.d.	n.d.
$t(1/2)$ [s]			n.d.	n.d.
VC	4.5 \pm 0.4	6.5 \pm 0.4**	n.d.	n.d.
VD	8.5 \pm 1.2	9.8 \pm 0.5	n.d.	n.d.

resolution. Use of this novel system will reduce the number of mice required, because experiments can be carried out at multiple time points with the same animal. Furthermore, the many transgenic and knock-out mouse strains available makes this model a very useful tool for biomedical research. High-resolution OCT systems facilitate the characterization of vascular structure and function. Further development of an OCT system with higher acquisition rates will enable Doppler OCT measurement^{17,18} of blood flow in different vessel types throughout the entire cardiac cycle. Based on blood flow data, the blood velocity and the biomechanical stress it imparts to the vascular wall can be calculated. Higher acquisition rates may also reveal time-resolved changes of inner diameter and wall thickness caused by the heartbeat (600 bpm), thus contributing to our understanding of vascular wall elastic properties. Our innovative *in-vivo* application of FD-OCT in the mouse model will be an attractive alternative to classic isometric force measurements for investigating vascular function and dynamics.

Acknowledgments

This study was supported by grants from MeDDrive38 programs 2007 and 2008 of the Faculty of Medicine Carl Gustav Carus of the Dresden University of Technology (Müller), the German Federal Ministry of Education and Research (BMBF) program NBL3 of the Dresden University of Technology (Morawietz, Professorship of Vascular Endothelium and Microcirculation; Koch, Professorship of Clinical Sensing and

Monitoring). We are grateful to Mirko Mehner for excellent technical assistance and to Dana Niegsch for proofreading the manuscript.

References

- Guidelines subcommittee, "World Health Organization-International Society of Hypertension guidelines for the management of hypertension," *J. Hypertens.* **17**, 151–183 (1999).
- P. K. Shah, "Mechanisms of plaque vulnerability and rupture," *J. Am. Coll. Cardiol.* **41**(4), 15–22 (2003).
- E. Falk, P. K. Shah, and V. Fuster, "Coronary plaque disruption," *Circulation* **92**(3), 657–671 (1995).
- P. Greenland, S. S. Gidding, and R. P. Tracy, "Commentary: lifelong prevention of atherosclerosis: the critical importance of major risk factor exposures," *Int. J. Epidemiol.* **31**(6), 1129–1134 (2002).
- R. Ross, "Atherosclerosis-an inflammatory disease," *N. Engl. J. Med.* **340**(2), 115–126 (1999).
- G. K. Hansson, "Inflammation, atherosclerosis, and coronary artery disease," *N. Engl. J. Med.* **352**(16), 1685–1695 (2005).
- Y. S. Chatzizisis, A. U. Coskun, M. Jonas, E. R. Edelman, C. L. Feldman, and P. H. Stone, "Role of endothelial shear stress in the natural history of coronary atherosclerosis and vascular remodeling," *J. Am. Coll. Cardiol.* **49**, 2379–2393 (2007).
- A. F. Fercher, W. Drexler, C. K. Hitzenberger, and T. Lasser, "Optical coherence tomography-principles and applications," *Rep. Prog. Phys.* **66**(2), 239–303 (2003).
- J. A. Schaar, F. Mastik, E. Regar, C. A. den Uil, F. J. Gijssen, J. J. Wentzel, P. W. Serruys, and A. F. van der Stehen, "Current diagnostic modalities for vulnerable plaque detection," *Curr. Pharm. Des.* **13**(10), 995–1001 (2007).
- J. A. Angus and C. E. Wright, "Techniques to study the pharmacodynamics of isolated large and small blood vessels," *J. Pharmacol. Toxicol. Methods* **44**(2), 395–407 (2000).
- G. Haeusler and M. W. Lindner, "Coherence radar and spectral radar new tools for dermatological diagnosis," *J. Biomed. Opt.* **3**(1), 21–31 (1998).
- S. H. Yun, G. J. Tearney, J. F. de Boer, and B. E. Bouma, "Motion artefacts in optical coherence tomography with frequency-domain ranging," *Opt. Express* **12**(13), 2977–2998 (2004).
- J. Walther, A. Krueger, M. Cuevas, and E. Koch, "Effects of axial, transverse and oblique sample motion in FD OCT in systems with global or rolling shutter line detector," *J. Opt. Soc. Am. A* **25**(11), 2791–2802 (2008).
- P. Gaetgens, "Das Kreislaufsystem," Chap. 8 in *Lehrbuch der Physiologie*, 3. Aufl., R. Klinke and S. Silbernagl, Eds., pp. 145–188, Thieme, Stuttgart, New York (2001).
- K. Holemans, R. Gerber, K. Meurrens, F. De Clerck, L. Poston, and F. A. Van Assche, "Maternal food restriction in the second half of pregnancy affects vascular function but not blood pressure of rat female offspring," *Br. J. Nutr.* **81**(1), 73–79 (1999).
- R. L. Van Citters, B. M. Wagner, and R. F. Rushmer, "Architecture of small arteries during vasoconstriction," *Circ. Res.* **10**, 668–675 (1962).
- C. J. Chang and K. H. Hou, "High-resolution optical Doppler tomography for in vitro and in vivo fluid flow dynamics," *Chang Keng I Hsueh* **26**(6), 403–411 (2003).
- J. Walther, G. Mueller, H. Morawietz, and E. Koch, "Analysis of in vitro and in vivo bidirectional flow velocities by phase-resolved Doppler Fourier-domain OCT," *Sens. Actuators, A* (in press).